Journal of Brilliant Engineering 4 (2026) 41149
Brilliant Engineering
journal home: www.acapublishing.com/journals/4/ben

Research Article

# Enhanced Photocatalytic Degradation of Methylene Blue Using a $BiVO_4/WO_3$ Composite Modified with Cobalt-Containing Species

Fadi Hasan,[1], Taner Tekin[*,2]
[1,2]*Department of Chemical Engineering, Atatürk University, Erzurum, Türkiye*

**Keywords**

*Photocatalytic degradation, $BiVO_4/WO_3$ composite doped with cobalt-containing species, Methylene blue, Hydrothermal synthesis, Pseudo-First-Order Kinetic Model, Pseudo-Second-Order Kinetic Model.*

**Abstract**

In recent years, considerable attention has been devoted to developing sustainable, cost-effective, and environmentally friendly composites for the removal of organic pollutants from aqueous media. Among semiconductor photocatalysts, $BiVO_4$ has attracted significant interest due to its favorable physicochemical properties and potential application in photocatalytic processes. In this study, $BiVO_4/WO_3$ composite doped with cobalt-containing species loadings were synthesized via a hydrothermal method to investigate the effect of cobalt-containing species addition on methylene blue (MB) degradation. The morphological and crystalline structures of the synthesized composites were characterized using scanning electron microscopy coupled with energy-dispersive spectroscopy (SEM-EDS) and X-ray diffraction (XRD). EDS analysis confirmed the presence of oxygen, bismuth, vanadium, tungsten, and cobalt within the composite structure. Photocatalytic degradation experiments were performed under UV-C irradiation (254 nm, 44 W $m^{-2}$) using methylene blue as a model pollutant. Among the samples examined, the $BiVO_4/WO_3$ photocatalyst containing 0.5% by weight Co-dopant showed the highest degradation efficiency, achieving 61% MB removal after 120 minutes. In comparison, $BiVO_4/WO_3$/1 wt% Co-dopant, $BiVO_4/WO_3$, $BiVO_4/WO_3$/1.5 wt% Co-dopant, and $BiVO_4/WO_3$/2wt% Co-dopant showed removal efficiencies of 45%, 35%, 28%, and 6%, respectively. The results suggest that moderate loading of cobalt-containing species is associated with enhanced photocatalytic degradation performance under the conditions investigated, whereas excessive loading adversely affects MB removal efficiency.

## 1. Introduction

The persistence, chemical stability, and toxicity of synthetic organic dyes released into industrial wastewater pose serious environmental concerns. Their resistance to biodegradation and complex aromatic structures makes removal by conventional treatment methods difficult [1, 2]. Among these pollutants, methylene blue (MB) is widely used in textile, paper, printing, and dyeing industries and is frequently employed as a model organic contaminant because of its stable aromatic structure and resistance to degradation [2, 3]. Therefore, the development of sustainable, economical, and efficient remediation technologies for removing dye pollutants has become increasingly important [4, 5].

Semiconductor-based photocatalysis has emerged as a promising advanced oxidation process for wastewater treatment due to its ability to generate highly reactive species that degrade persistent organic contaminants into less harmful products [6, 7]. When irradiated with photons whose energy exceeds the semiconductor band gap, electrons are excited from the valence band to the conduction band, forming photogenerated electron-hole pairs. These charge carriers may subsequently participate in oxidation and reduction reactions, producing reactive oxygen species such as hydroxyl radicals (•OH) and superoxide radicals ($•O_2^-$), which play important roles in pollutant degradation [8, 9]. However, the rapid recombination of photogenerated charge carriers remains one of the major limitations that reduces photocatalytic efficiency.

Among semiconductor photocatalysts, bismuth vanadate ($BiVO_4$) has attracted considerable attention owing to its favorable physicochemical properties, suitable band structure, and good stability in aqueous environments [10, 11]. Tungsten trioxide ($WO_3$), due to its strong oxidative capability, structural stability, and favorable electronic properties, is also considered a suitable component in composite photocatalytic systems [12-14]. Constructing composite structures between semiconductor materials may facilitate interfacial charge transfer, improve charge carrier separation, and suppress recombination losses, thereby enhancing photocatalytic performance [15-17].

In recent years, transition-metal oxide cocatalysts have attracted increasing interest for improving photocatalytic systems. Among them, Co-dopant is considered a promising cocatalyst due to its favorable redox characteristics, catalytic activity, and ability to provide additional active surface sites for photocatalytic reactions [18, 19]. The incorporation of cobalt-containing species into composite systems may improve interfacial electron transfer and promote surface redox reactions. However, excessive cocatalyst loading may lead to particle agglomeration, surface coverage, or the formation of additional recombination centers, which can adversely affect photocatalytic activity [20-25].

Although $BiVO_4/WO_3$-based photocatalytic systems have been investigated in previous studies, the specific role of cobalt-containing species as a cocatalyst and the influence of cobalt-containing species loading on photocatalytic degradation efficiency remain insufficiently understood. In particular, systematic studies on optimizing cobalt-containing species loading in $BiVO_4/WO_3$ composite systems for dye degradation remain limited. Therefore, determining the optimum cobalt-containing species loading is essential for maximizing catalyst performance and understanding its contribution to photocatalytic activity.

*Corresponding Author: ttekin@atauni.edu.tr
Received 25 May 2026; Revised 12 Aug 2026; Accepted 14 Aug 2026
https://doi.org/10.36937/ben.2026.41149

In this study, cobalt-containing species-modified $BiVO_4/WO_3$ composite were synthesized using a hydrothermal method. The morphological and crystalline properties of the synthesized composites were investigated using SEM-EDS and X-ray diffraction (XRD) analyses. The photocatalytic performance of the prepared samples was evaluated through methylene blue degradation under UV irradiation, and concentration changes were monitored using UV–Vis spectroscopy.

## 2. Materials and methods

### 2.1. Materials

Sodium tungstate dihydrate ($Na_2WO_4{\cdot}2H_2O$, Sigma-Aldrich, ≥ 99%), sodium chloride (NaCl, Sigma-Aldrich, ≥ 99%), hydrochloric acid (HCl, Sigma-Aldrich, 37%), bismuth (III) nitrate pentahydrate ($Bi(NO_3)_3{\cdot}5H_2O$, Sigma-Aldrich, 98%), vanadium (V) oxide ($V_2O_5$, Merck, 99%), potassium sulfate ($K_2SO_4$, Sigma-Aldrich, ≥ 99%), and sodium hydroxide (NaOH, Sigma-Aldrich, ≥ 98%) were obtained from the respective suppliers. For the preparation of Co-dopant, precursor reagents, specifically ammonium fluoride ($NH_4F$, Sigma-Aldrich, ≥ 98%), urea ($CO(NH_2)_2$, Sigma-Aldrich, ≥ 98%), and cobalt nitrate hexahydrate ($Co(NO_3)_2{\cdot}6H_2O$, Sigma-Aldrich, ≥ 98%), were employed as precursor material. Potassium iodide (KI, Sigma-Aldrich, ≥ 99%), benzoquinone (BQ, Sigma-Aldrich, ≥ 98%), potassium bromate ($KBrO_3$, Sigma-Aldrich, ≥ 99.8%), and isopropanol (IPA, $(CH_3)_2CHOH$, Sigma-Aldrich, ≥ 99.5%) were used as scavengers in reactive species-trapping experiments. Deionized water (DI) was used throughout all stages of the experimental work. In addition, MB ($C_{16}H_{18}ClN_3S$, Sigma-Aldrich, ≥ 82%) was used as a model dye in the photocatalytic activity experiments to determine the optimum cobalt oxide loading.

### 2.2. Synthesis of $BiVO_4$

$BiVO_4$ was synthesized via a hydrothermal method. Briefly, 1.455 g of $Bi(NO_3)_3{\cdot}5H_2O$, 0.555 g of $V_2O_5$, and 15 g of $K_2SO_4$ were dispersed in 150 mL of deionized water. The mixture was magnetically stirred until a homogeneous solution was obtained. The resulting solution was transferred into a Teflon-lined stainless-steel autoclave and heated at 200 °C for 24 h. After completion of the hydrothermal reaction, the autoclave was allowed to cool naturally to room temperature. The resulting precipitate was collected by filtration and washed several times with distilled water to remove residual impurities. After drying at 90 °C, the obtained powder was calcined at 550 °C for 2 h to obtain crystalline $BiVO_4$ particles.

### 2.3. Synthesis of $WO_3$

$WO_3$ was synthesized via a hydrothermal method. Briefly, 6.579 g of $Na_2WO_4{\cdot}2H_2O$ and 2.3128 g of NaCl were dissolved in deionized water under continuous magnetic stirring until a clear solution was obtained. The pH of the solution was adjusted to 2 using 3 M HCl. The resulting solution was transferred into a Teflon-lined stainless-steel autoclave and heated at 180°C for 24 h. After the hydrothermal reaction, the autoclave was allowed to cool naturally to room temperature. The precipitate was collected by filtration, thoroughly washed with deionized water, and dried at 90 °C. Finally, the dried powder was calcined at 520 °C for 2 h to obtain $WO_3$.

### 2.4. Synthesis of $BiVO_4/WO_3$ composite doped with cobalt-containing species

$BiVO_4/WO_3$ composite doped with cobalt-containing species was synthesized via a hydrothermal method. Predetermined amounts of $BiVO_4$ and $WO_3$ (according to Table 1) were dispersed in deionized water and magnetically stirred for 10 min to obtain a homogeneous slurry. Subsequently, the calculated amounts of cobalt-containing species precursor materials, namely $NH_4F$, $CO(NH_2)_2$, and $Co(NO_3)_2{\cdot}6H_2O$, were added to the suspension, followed by an additional 10 min of magnetic stirring. The resulting mixture was then ultrasonicated for 10 min to ensure uniform dispersion.

The prepared suspension was transferred into a Teflon-lined autoclave and heated at 110 °C for 6 h. After completion of the hydrothermal reaction, the autoclave was allowed to cool naturally to room temperature. The resulting solid product was collected by filtration and washed several times to remove residual impurities. The obtained material was dried at 60 °C and subsequently calcined at 300 °C for 2 h to obtain the final $BiVO_4/WO_3$ composite doped with a cobalt-containing species photocatalyst.

As shown in Table 1, cobalt-containing species loadings ranging from 0 to 2 wt% were evaluated to determine the optimum loading amount.

Table 1. Composition of $BiVO_4/WO_3$ composite with types containing different amounts of cobalt (0–2 wt%)

| Sample | Co-dopant (wt%) | $WO_3$ (mg) | $BiVO_4$ (mg) | Co-dopant (mg) | Co-dopant (mmol) | $Co(NO_3)_2{\cdot}6H_2O$ (mg) | Urea (mg) | $NH_4F$ (mg) | Total (g) |
|---|---|---|---|---|---|---|---|---|---|
| F1 | 0 | 416.7 | 583.3 | 0 | 0.000 | 0.00 | 0.00 | 0.00 | 1.000 |
| F2 | 0.5 | 414.6 | 580.4 | 5 | 0.067 | 19.42 | 20.04 | 2.47 | 1.000 |
| F3 | 1.0 | 412.5 | 577.5 | 10 | 0.133 | 38.84 | 40.08 | 4.94 | 1.000 |
| F4 | 1.5 | 410.4 | 574.6 | 15 | 0.200 | 58.26 | 60.11 | 7.41 | 1.000 |
| F5 | 2.0 | 408.3 | 571.7 | 20 | 0.267 | 77.68 | 80.15 | 9.89 | 1.000 |

To prepare the sample without cobalt oxide, $BiVO_4$ and $WO_3$ were mixed by magnetic stirring for 10 min, then ultrasonicated for an additional 10 min. Subsequently, the same hydrothermal treatment, drying, and calcination procedures were applied.

### 2.5. Characterization

The morphological, elemental, and crystalline properties of the synthesized samples were characterized using scanning electron microscopy coupled with energy-dispersive spectroscopy (SEM-EDS, Zeiss Sigma 300) and X-ray diffraction (XRD, Rigaku SmartLab). XRD measurements were performed using Cu-Kα radiation (λ = 1.5406 Å) over a 2θ range of 10–90°. Photoluminescence (PL) analysis was performed at room temperature between 325-1000 nm. Analyses were performed using a Si photodetector with a wavelength range of 300–1000 nm.

### 2.6. Photocatalytic degradation of methylene blue

The photocatalytic activity of $BiVO_4/WO_3$ composite doped with cobalt-containing species was evaluated by degrading MB in aqueous solution. Photocatalytic experiments were carried out using a low-pressure mercury vapor UV lamp operating in the UV-C region (254 nm, 44 W $m^{-2}$) as the irradiation source. Experimental conditions included an initial MB concentration of 20 mg/L, a solution volume of 400 mL, a catalyst dosage of 100 mg, and a reaction temperature of 25 °C.

Photocatalytic recycling experiments were performed independently in multiple replicates (n=10). After the dye degradation experiment was completed, the catalysts were separated from the dye by centrifugation (4000 rpm, 10 min). The catalysts were then washed several times with DI to remove the dyes and dried at 60 °C. The parameters for the recycling experiments were determined to be the same as those for the photocatalytic activity experiments. Before irradiation, the suspension was magnetically stirred in the dark for 30 min to establish adsorption–desorption equilibrium between the catalyst surface and MB molecules. Air was continuously supplied to the reaction system using an $O_2$ pump to maintain sufficient dissolved oxygen during photocatalysis. During the degradation experiments, samples were collected at 5 min intervals during the initial stage and subsequently at 15 min intervals. The concentration of MB was determined using a UV–Vis spectrophotometer (Optizen α) at λmax = 668 nm.

For scavenger experiments performed on the cobalt-containing species-modified $BiVO_4/WO_3$ composite, all experimental parameters were kept identical to those used in the photocatalytic degradation experiments. Each scavenger was sequentially introduced into the reaction medium at a fixed concentration of 1 mM to evaluate the contributions of different reactive species during the photocatalytic degradation process.

## 3. Results and discussion

### 3.1. SEM and EDS studies

SEM images of the synthesized $BiVO_4/WO_3$, $BiVO_4/WO_3$/0.5% Co-dopant, $BiVO_4/WO_3$/1% Co-dopant, $BiVO_4/WO_3$/1.5% Co-dopant, and $BiVO_4/WO_3$/2% Co-dopant composites are presented in Figure 1, providing insight into the surface morphology and microstructural characteristics of the prepared composite samples.

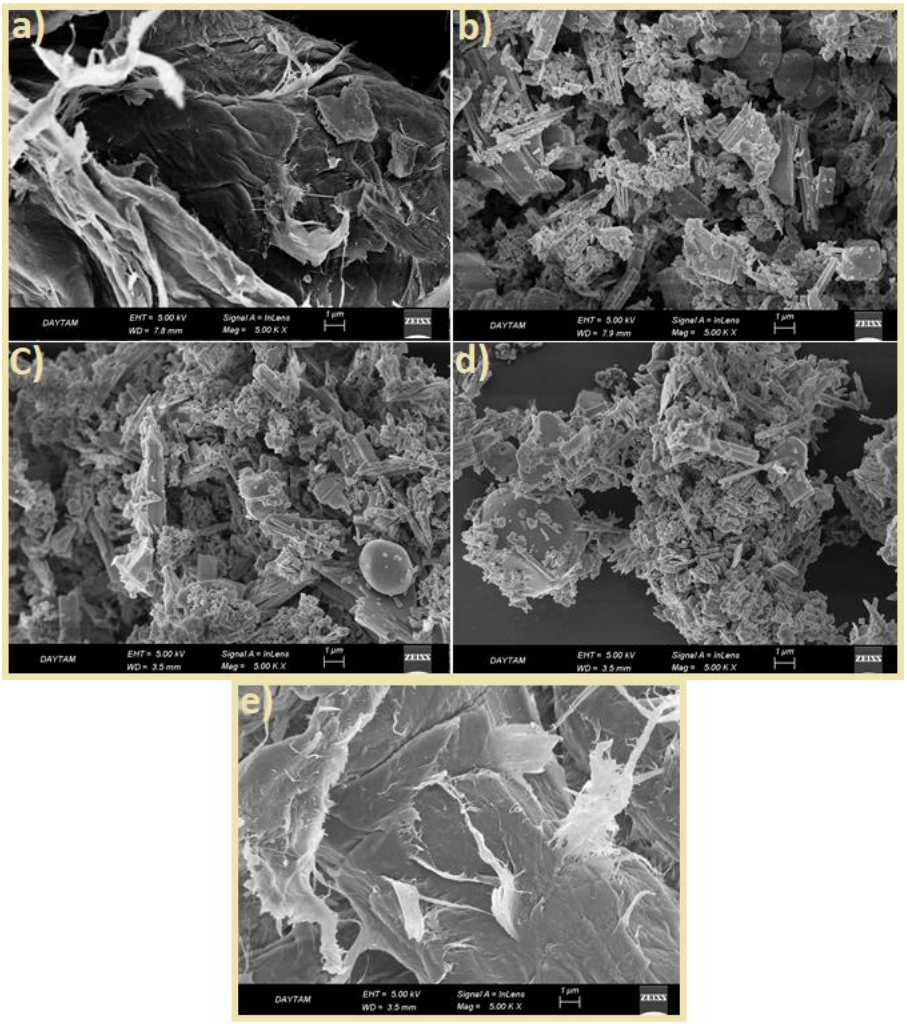


Figure 1. SEM images of the synthesized composites: a) $BiVO_4/WO_3$, b) $BiVO_4/WO_3$/0.5% Co-dopant, c) $BiVO_4/WO_3$/1% Co-dopant, d) $BiVO_4/WO_3$/1.5% Co-dopant, and e) $BiVO_4/WO_3$/2% Co-dopant

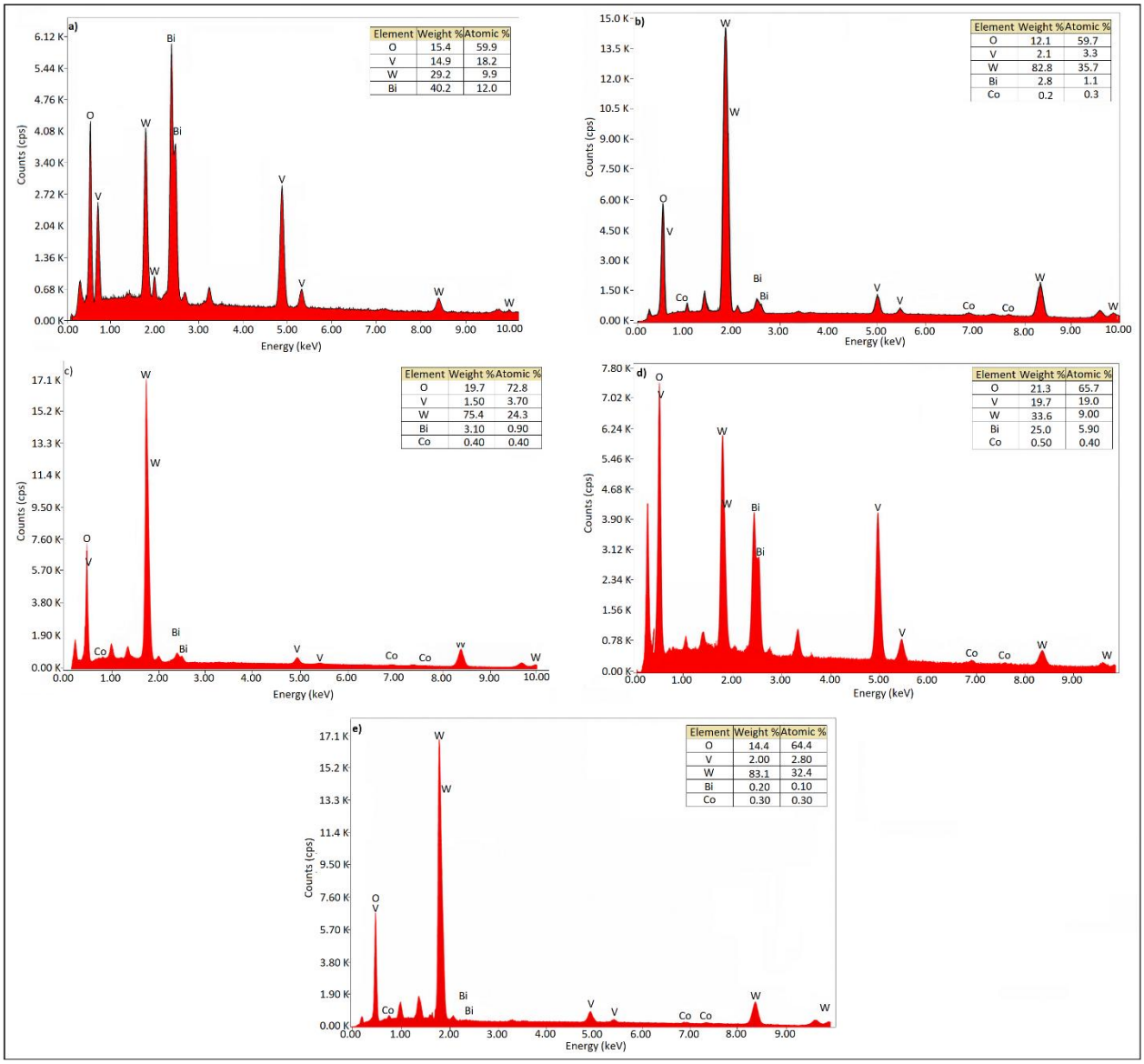


Figure 2. EDS spectra of the synthesized composites: a) $BiVO_4/WO_3$, b) $BiVO_4/WO_3$/0.5% Co-dopant, c) $BiVO_4/WO_3$/1% Co-dopant, d) $BiVO_4/WO_3$/1.5% Co-dopant and e) $BiVO_4/WO_3$/2% Co-dopant

As presented in Figure 1, all synthesized samples exhibited heterogeneous composite morphologies with noticeable particle agglomeration. The $BiVO_4/WO_3$ sample (Figure 1a) mainly displayed plate-like and layered structures with relatively compact domains. After cobalt-containing species modification (Figures 1b–d), additional fine particles and agglomerated domains were observed on the composite surface, indicating morphological changes associated with cobalt incorporation. These structural changes suggest increased interfacial contact between the constituent phases.

Rod-like crystallites observed in the SEM images may correspond to $BiVO_4$-rich regions, whereas flat and irregular plate-like structures may be associated with $WO_3$-rich domains, consistent with morphologies reported in previous studies [26]. In the cobalt-containing species modified samples, small, granular, nearly spherical particles were also observed, which may be attributed to cobalt-containing species dispersed within the composite matrix. The presence of these particles suggests that cobalt-containing species were successfully introduced into the $BiVO_4/WO_3$ composite structure.

Among the synthesized samples, the 0.5 wt% Co-dopant composite exhibited a relatively well-dispersed morphology with limited agglomeration, which may favor improved surface interaction and photocatalytic activity. In contrast, increasing cobalt-containing species loading beyond this level resulted in more pronounced agglomeration and partial coverage of surface-active regions. Particularly, the 2 wt% Co-dopant sample (Figure 1e) exhibited a more compact and sheet-like morphology similar to the undoped sample, suggesting that excessive cobalt-containing species loading may reduce accessible active sites and hinder photocatalytic performance.

As shown in Figure 2, EDS spectra confirmed the presence of oxygen, bismuth, vanadium, tungsten, and cobalt in the synthesized composites, supporting the successful incorporation of cobalt-containing species into the $BiVO_4/WO_3$ matrix. The appearance of cobalt peaks in cobalt-containing species-modified samples further supports cobalt incorporation. However, since EDS analysis provides localized compositional information, quantitative variations in elemental percentages should be interpreted with caution.

Figure 3 presents the XRD patterns of $BiVO_4/WO_3$, $BiVO_4/WO_3$/0.5% Co-dopant, $BiVO_4/WO_3$/1% Co-dopant, $BiVO_4/WO_3$/1.5% Co-dopant and $BiVO_4/WO_3$/2% Co-dopant composites.

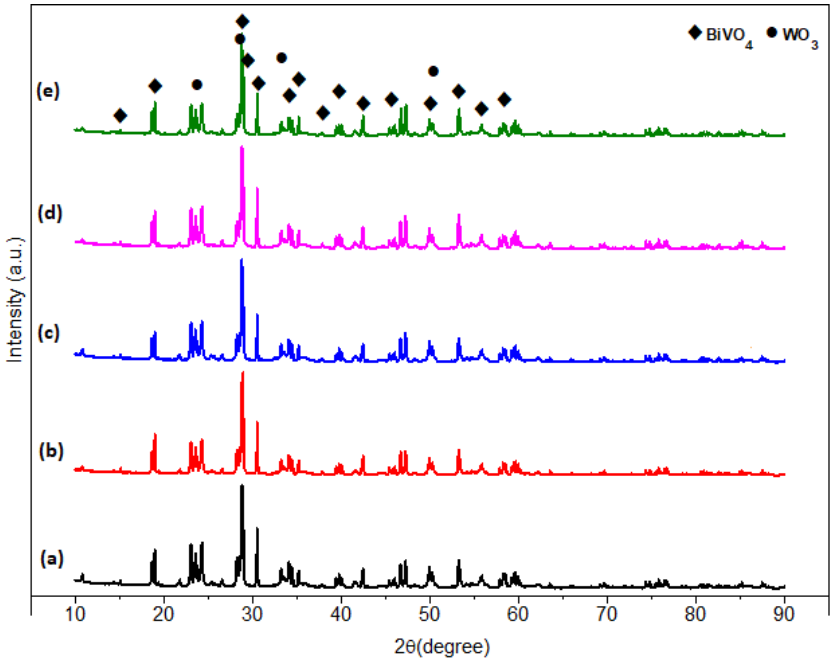


Figure 3. XRD patterns of (a) $BiVO_4/WO_3$, (b) $BiVO_4/WO_3$/0.5% Co-dopant, (c) $BiVO_4/WO_3$/1% Co-dopant, (d) $BiVO_4/WO_3$/1.5% Co-dopant and (e) $BiVO_4/WO_3$/2% Co-dopant composites

Figure 3 presents the XRD patterns of $BiVO_4/WO_3$, $BiVO_4/WO_3$/0.5% Co-dopant, $BiVO_4/WO_3$/1% Co-dopant, $BiVO_4/WO_3$/1.5% Co-dopant and $BiVO_4/WO_3$/2% Co-dopant composites. The diffraction peaks observed at approximately 18.8°, 28.9°, 30.5°, 34.5°, 35.2°, 39.8°, 42.4°, 46.7°, and 53.3° can be indexed to the characteristic crystal planes of monoclinic scheelite $BiVO_4$ (JCPDS card no. 14-0688), confirming the formation of crystalline $BiVO_4$ [27]. In addition, diffraction peaks observed around 23–24°, 26–27°, 33–34°, 41–42°, 49–50°, and 55–56° are consistent with monoclinic $WO_3$ (JCPDS card no. 43-1035), indicating the successful incorporation of $WO_3$ into the composite structure [26].

After cobalt-containing species modification, no significant peak shift or structural distortion was observed, indicating that the crystal structures of $BiVO_4$ and $WO_3$ remained largely unchanged. Furthermore, no distinct diffraction peaks corresponding to crystalline cobalt-containing species were detected. Characteristic diffraction peaks of cubic cobalt-containing species are generally expected near 36.5°, 42.4°, 61.5°, and 73.7° (JCPDS card no. 48-1719) [28]. The absence of clearly distinguishable cobalt-containing species peaks may be attributed to the relatively low cobalt-containing species loading (0.5–2 wt%), high dispersion of cobalt-containing species on the composite surface, and/or overlap of cobalt-containing species reflections with the dominant $BiVO_4$ and $WO_3$ diffraction peaks. These results suggest that cobalt-containing species incorporation did not significantly alter the crystalline framework of the $BiVO_4/WO_3$ composite [29].

Figure 4 shows the PL spectra of $BiVO_4/WO_3$, $BiVO_4/WO_3$/0.5% Co-dopant, $BiVO_4/WO_3$/1% Co-dopant, $BiVO_4/WO_3$/1.5% Co-dopant, and $BiVO_4/WO_3$/2% Co-dopant composites.

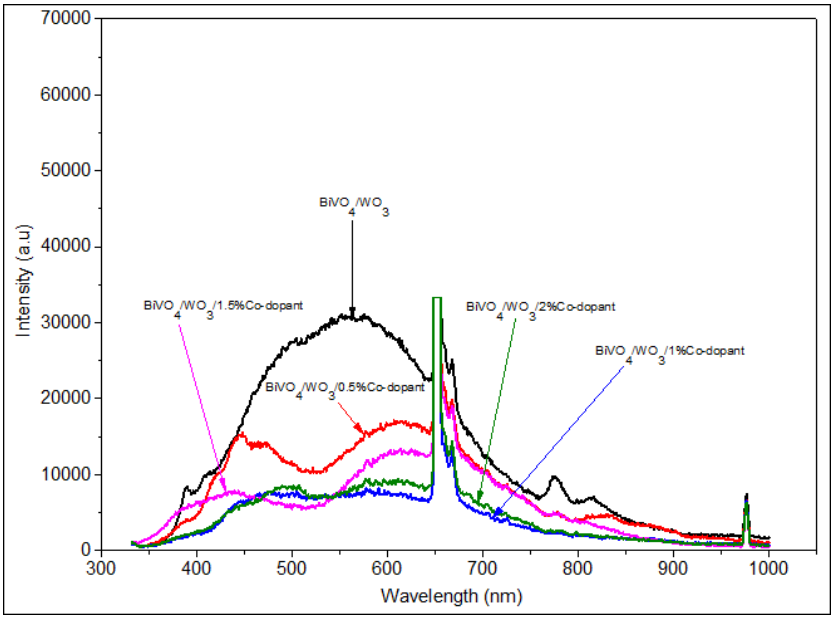


Figure 4. PL spectra of $BiVO_4/WO_3$, $BiVO_4/WO_3$/0.5% Co-dopant, $BiVO_4/WO_3$/1% Co-dopant, $BiVO_4/WO_3$/1.5% Co-dopant and $BiVO_4/WO_3$/2% Co-dopant composites

The PL spectrum shown in Figure 4 exhibits emission bands at 443, 496, 615, and 773 nm. A scattering-related peak is observed around 625 nm. Co-doped composites suppress PL emission and inhibit electron-hole pair recombination compared to the pure $BiVO_4/WO_3$ composite. The 0.5% weight Co-doped $BiVO_4/WO_3$ composite, exhibiting a 61% degradation percentage, shows high degradation behavior towards methylene blue dye, while a decrease in PL intensity is observed. This is thought to be due to the 0.5% Co doping leading to an optimum concentration and improving charge separation. Adding 1% and 1.5% Co to the $BiVO_4/WO_3$ composite resulted in a decrease in PL intensity but did not lead to a photocatalytic improvement. This suggests that the degradation efficiency is affected by parameters such as the presence of accessible catalytic sites, interfacial charge transfer, adsorption of reactant molecules, and synergistic interactions during charge dissociation. Therefore, judging photocatalytic performance solely by PL peaks is insufficient. Finally, considering the 2% Co addition, excessive Co doping reduces the effective participation of redox reactions occurring on the surface of photon-generating charge carriers by covering the active surfaces of the $BiVO_4/WO_3$ composite. According to PL results, composites with high Co doping have lower photocatalytic activity compared to those with 0.5% Co doping.

### 3.2. Photocatalytic (PC) activity characteristics of composites

The Time-Concentration graph of composites with Dark medium, without catalyst, $BiVO_4$, $WO_3$, $BiVO_4/WO_3$, $BiVO_4/WO_3$/0.5% Co-dopant, $BiVO_4/WO_3$/1% Co-dopant, $BiVO_4/WO_3$/1.5% Co-dopant, and $BiVO_4/WO_3$/2% Co-dopant after 120 minutes is shown in Figure 5. Furthermore, the error bars (n=10) shown in Figure 5 were calculated from the results of repeated recycling. The methylene blue removal percentages of the synthesized composites and the standard deviation values calculated from the recycling results obtained by reconstruction (n=10) are given in Table 2.

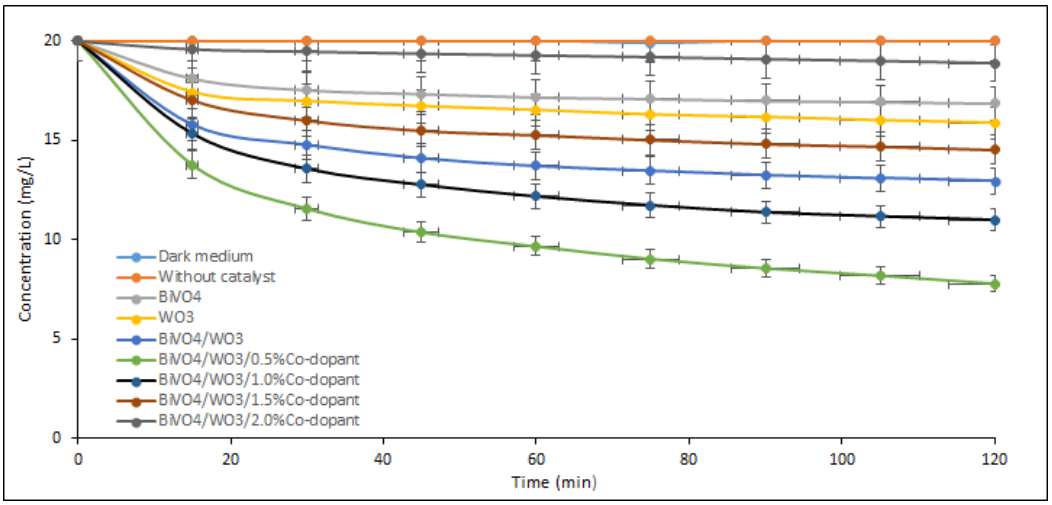


Figure 5. Time-concentration graph of methylene blue degradation of Dark medium, without catalyst, $BiVO_4$, $WO_3$, $BiVO_4/WO_3$, $BiVO_4/WO_3$/0.5% Co-dopant, $BiVO_4/WO_3$/1% Co-dopant, $BiVO_4/WO_3$/1.5% Co-dopant, and $BiVO_4/WO_3$/2% Co-doped composites within 120 minutes, and error bars showing the standard deviation of ten independent (n=10) replicates.

Table 2. Methylene blue removal percentages and standard deviations of recovery values obtained after 10 replicates for dark medium, without catalyst, $BiVO_4$, $WO_3$, $BiVO_4/WO_3$, $BiVO_4/WO_3$/0.5% doped, $BiVO_4/WO_3$/1% doped, $BiVO_4/WO_3$/1.5% doped, and $BiVO_4/WO_3$/2% doped composites

| Samples | Photocatalytic activity efficiency (%) | SD (±) |
|---|---|---|
| Dark medium | 0.095 | 0.00127 |
| Without catalyst | 0.105 | 0.00158 |
| $BiVO_4$ | 15.74 | 0.9978 |
| $WO_3$ | 20.725 | 0.9503 |
| $BiVO_4/WO_3$ | 35.215 | 1.0024 |
| $BiVO_4/WO_3$/0.5% Co-dopant | 61.075 | 1.0185 |
| $BiVO_4/WO_3$/%1 Co-dopant | 45.09 | 1.0137 |
| $BiVO_4/WO_3$/1.5% Co-dopant | 27.38 | 0.9269 |
| $BiVO_4/WO_3$/2% Co-dopant | 5.635 | 0.3983 |

As shown in Figure 5, the photocatalytic degradation profiles of MB over $BiVO_4$, $WO_3$, $BiVO_4/WO_3$, $BiVO_4/WO_3$/0.5%Co-dopant, $BiVO_4/WO_3$/1% Co-dopant, $BiVO_4/WO_3$/1.5%Co-dopant, and $BiVO_4/WO_3$/2%Co-dopant composites were monitored for 120 min under UV irradiation, while the corresponding removal efficiencies are summarized in Table 2. Among all synthesized samples, the $BiVO_4/WO_3$/0.5%Co-dopant photocatalyst exhibited the highest photocatalytic activity, with the MB concentration decreasing from approximately 20 mg/L to about 7 mg/L after 120 min, corresponding to approximately 61% dye removal.

In experiments conducted in the dark and without a catalyst, the occurrence of the photocatalytic reaction is at a low level. Therefore, the variation between recycling repeats in experiments conducted in light-free and catalyst-free environments is generally small. In standard deviation experiments, the sample with 0.5% Co additive shows good photocatalytic activity compared to other samples and its stability is observed to be good after n=10 repeats. Before UV irradiation, the dye solution was stirred in the dark for 30 minutes to ensure adsorption-desorption equilibrium. A negligible change in MB concentration was observed in the dark. This indicates minimal dye adsorption on the catalyst surface, suggesting that the concentration change was due to photocatalytic degradation. The $BiVO_4/WO_3$/1% Co-dopant sample exhibited the second-highest photocatalytic performance, achieving approximately 45% MB removal. In comparison, $BiVO_4$, $WO_3$, $BiVO_4/WO_3$, $BiVO_4/WO_3$/1.5% Co-dopant, and $BiVO_4/WO_3$/2.0% Co-dopant composites achieved removal efficiencies of approximately 16%, 21%, 35%, 28%, and 6%, respectively. These results indicate that the photocatalytic performance of the $BiVO_4/WO_3$ composite is highly sensitive to cobalt-containing species loading, with 0.5 wt% identified as the optimal loading under the conditions investigated.

Photocatalytic experiments were conducted using methylene blue dye to evaluate the photocatalytic performance of the synthesized composites under UV light. In recycling tests performed under the same experimental conditions, the composite showed good stability and reproducibility over 10 repeated cycles. The enhanced photocatalytic performance at low cobalt-containing species loading may be attributed to improved interfacial interactions and the availability of additional active surface sites. However, excessive cobalt-containing species loading resulted in a significant decline in photocatalytic activity. In particular, the poor performance of the 2 wt% Co-dopant sample suggests that excessive cobalt-containing species may promote particle agglomeration, partially block active surface regions, and introduce additional recombination centers. Under UV irradiation, photogenerated charge carriers may react with adsorbed oxygen and water molecules to generate reactive species responsible for MB degradation.

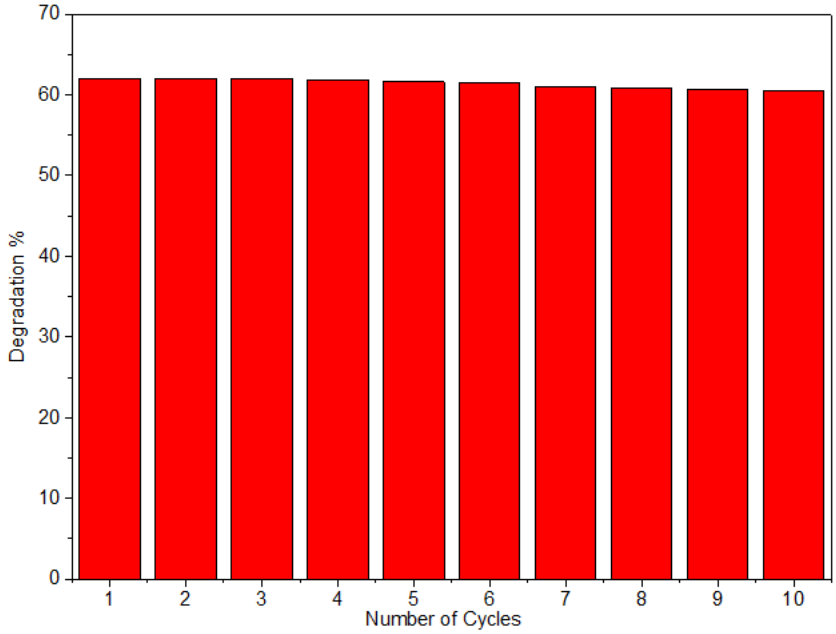


Figure 6. Photocatalytic stability of $BiVO_4/WO_3$/0.5% Co-dopant over 10 successive degradation cycles

As shown in Figure 6, the degradation efficiency of MB dye is over 60% after 10 repeated recycling cycles, indicating good reusability and stability. The slight decreases seen in the graph are likely due to surface contamination or minor catalyst losses during recovery.

As shown in Figure 7, scavenger experiments were performed to identify the dominant reactive species involved in the photocatalytic degradation process. KI, BQ, $KBrO_3$, and IPA were added separately to the reaction medium as scavengers for $h^+$, $\bullet O_2^-$, $e^-$, and •OH species, respectively. The photocatalytic degradation experiments on the $BiVO_4/WO_3$/0.5% Co-dopant composite were conducted under UV irradiation to evaluate the contribution of these reactive species to methylene blue degradation.

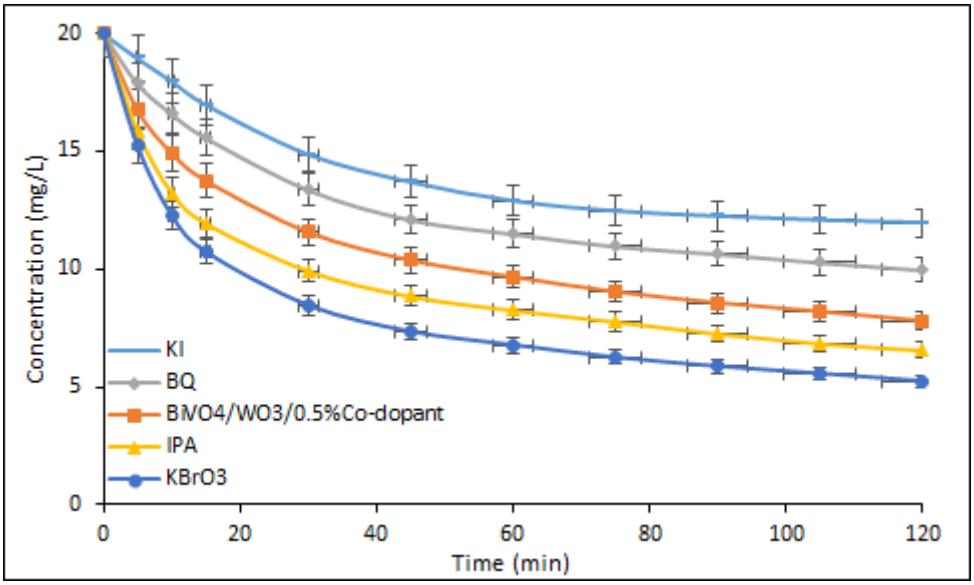


Figure 7. The effect of scavengers on the photocatalytic oxidation process of Methylene blue dye on $BiVO_4/WO_3$/0.5% Co-dopant composite

As shown in Figure 7, the addition of different scavengers significantly influenced the photocatalytic degradation of methylene blue, indicating that multiple reactive species participated in the degradation process. Among the scavengers tested, KI caused the greatest suppression of photocatalytic activity, resulting in the highest residual MB concentration after 120 min. Since KI acts primarily as a $h^+$ scavenger, this result suggests that photogenerated holes play a dominant role in the degradation mechanism.

The addition of BQ, a $\bullet O_2^-$ scavenger, also noticeably reduced photocatalytic performance, indicating that superoxide radicals contribute significantly to MB degradation. In contrast, the addition of IPA, a •OH scavenger, caused only limited inhibition, suggesting that hydroxyl radicals play a comparatively minor role in the photocatalytic process.

Interestingly, the addition of $KBrO_3$, an electron scavenger, enhanced photocatalytic degradation compared with the control sample. This behavior suggests that photogenerated electrons may act as recombination centers, and their consumption by $KBrO_3$ suppresses electron-hole recombination, thereby prolonging hole lifetime and enhancing photocatalytic efficiency. Based on these results, photogenerated holes ($h^+$) are identified as the dominant reactive species, while superoxide radicals ($\bullet O_2^-$) act as secondary contributors during methylene blue degradation.

The kinetic model applied to the $BiVO_4/WO_3$/0.5% Co-dopant sample in this study is expressed mathematically below.

Pseudo-first-order model: $ln(\frac{C_0}{C}) = kt$

Pseudo-second-order model: $\frac{1}{C} - \frac{1}{C_0} = kt$

where $C_0$ and C represent the initial and time-dependent concentrations of MB (mg $L^{-1}$), $k_1$ ($min^{-1}$), and $k_2$ (L $mg^{-1}min^{-1}$) are the rate constants of the respective models, and t is the reaction time (min). The photocatalytic degradation kinetics of methylene blue using the $BiVO_4/WO_3$/0.5% Co-dopant composite were evaluated using both pseudo-first-order and pseudo-second-order models. As shown in Figure 8, the kinetic data were linearly fitted to the respective kinetic models $ln(C_0/C)$ versus time for pseudo-first-order and $1/C-1/C_0$ versus time for pseudo-second-order.

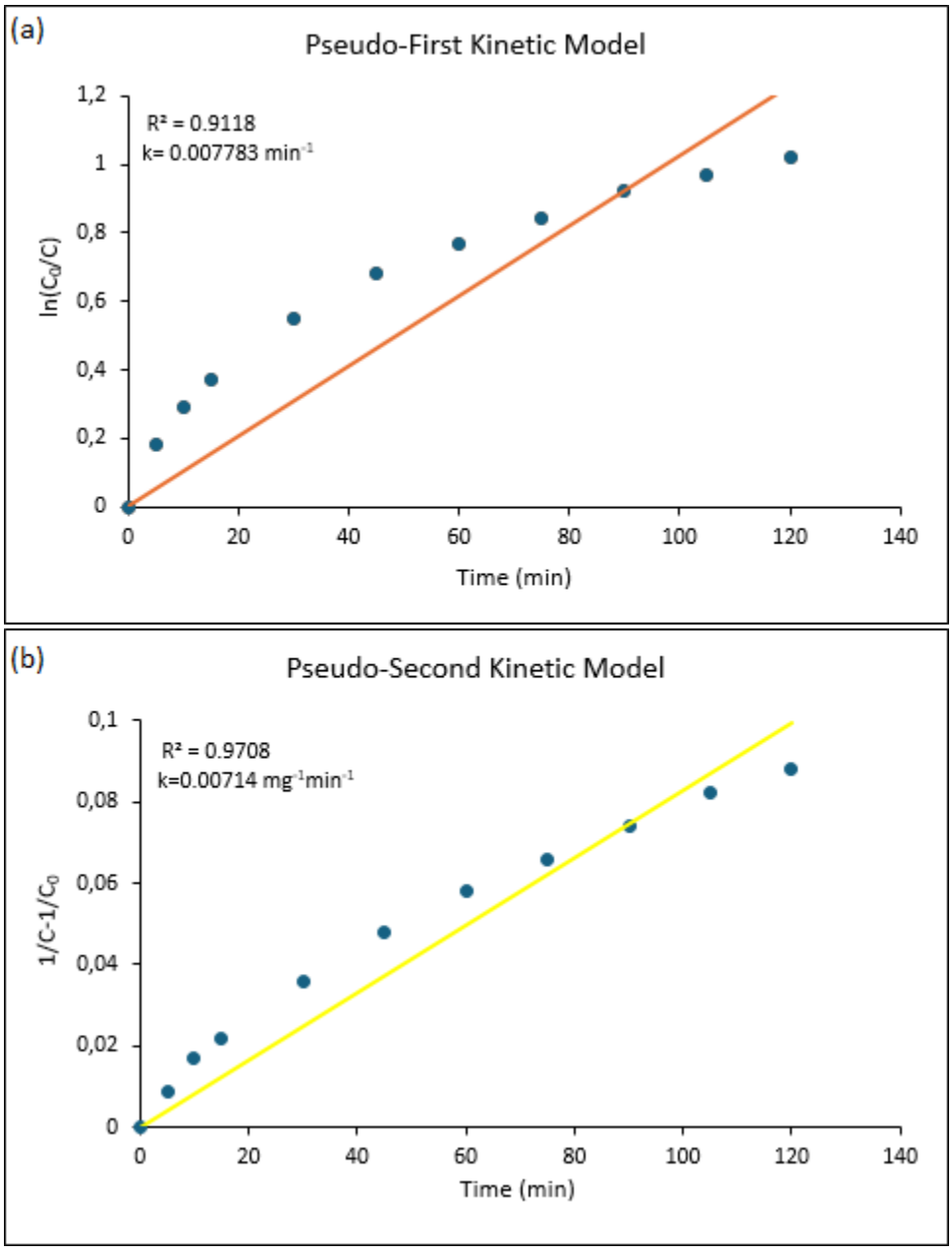


Figure 8. Kinetic modeling results: (a) pseudo-first-order and (b) pseudo-second-order linear fits for MB degradation using $BiVO_4/WO_3$/0.5% Co-dopant composite

Table 3. Calculated k and $R^2$ values of composites according to the first and second pseudo-kinetic models

| Samples | Pseudo-first-order kinetic model | | Pseudo-second-order kinetic model | |
|---|---|---|---|---|
| | $k_1$ ($min^{-1}$) | $R^2$ | $k_2$ ($mg^{-1}min^{-1}$) | $R^2$ |
| $BiVO_4$ | 0.001156 | 0.735990 | 0.000064 | 0.752783 |
| $WO_3$ | 0.001485 | 0.760767 | 0.000086 | 0.788016 |
| $BiVO_4/WO_3$ | 0.002987 | 0.781608 | 0.000195 | 0.824144 |
| $BiVO_4/WO_3$/0.5% Co-dopant | 0.007783 | 0.911786 | 0.000714 | 0.970892 |
| $BiVO_4/WO_3$/%1 Co-dopant | 0.004473 | 0.844368 | 0.000321 | 0.892094 |
| $BiVO_4/WO_3$/1.5% Co-dopant | 0.002330 | 0.776222 | 0.000142 | 0.804673 |
| $BiVO_4/WO_3$/2% Co-dopant | 0.000413 | 0.945204 | 0.000021 | 0.948687 |

As shown in Figure 8, the pseudo-second-order kinetic model exhibited a better linear fit, with a rate constant (k) of 0.00714 L $mg^{-1}$ $min^{-1}$ and a correlation coefficient ($R^2$) of 0.9708. In contrast, the pseudo-first-order kinetic model showed a poorer linear fit, with a rate constant (k) of 0.007783 $min^{-1}$ and a correlation coefficient ($R^2$) of 0.9118. These results demonstrate that the photocatalytic degradation of methylene blue (MB) on the $BiVO_4/WO_3$/0.5% Co-doped composite is best described by a pseudo-second-order kinetic model.

**4. Conclusion**

In this study, $BiVO_4/WO_3$ composite doped with cobalt-containing species with different cobalt-containing species loadings were successfully synthesized via a hydrothermal method, and their photocatalytic performance toward MB degradation under 254 nm UV-C irradiation was systematically investigated. SEM analysis revealed noticeable morphological changes after cobalt-containing species modification, while EDS confirmed the presence of cobalt-containing species in the composite structure. XRD analysis showed that the characteristic crystalline phases of $BiVO_4$ and $WO_3$ were preserved after cobalt-containing species incorporation, indicating that cobalt-containing species addition did not significantly alter the crystalline framework of the composite. PL analyses show that the addition of cobalt-containing species causes a change in the intensity of the peaks and that charge separation occurs in the samples. Photocatalytic degradation experiments demonstrated that cobalt-containing species loading significantly influenced photocatalytic performance under UV-C irradiation. Among all synthesized samples, the $BiVO_4/WO_3$/0.5 wt% Co-dopant photocatalyst exhibited the highest activity, achieving approximately 61% MB removal after 120 min, whereas higher cobalt-containing species loadings resulted in progressively lower degradation efficiencies. These findings demonstrate that small variations in cobalt-containing species loading substantially affect photocatalytic behavior under the applied experimental conditions. The enhanced performance at low cobalt-containing species loading may be attributed to improved interfacial interactions and the availability of additional active surface sites, while excessive cobalt-containing species loading likely promoted particle agglomeration and increased charge carrier recombination. Reactive species trapping experiments indicated that photogenerated holes ($h^+$) were the dominant reactive species responsible for MB degradation, while $\bullet O_2^-$ also contributed to the photocatalytic process.

## Declaration of Conflict of Interests

The authors declare no conflict of interest. They have no known competing financial interests or personal relationships that could have appeared to influence the work reported in this paper.

## Acknowledgement

This project (FYL-2026-17518) was supported by Atatürk University, Administration System of Scientific Research Project.

## References

[1.] Forgacs, E., T. Cserháti, and G. Oros, Removal of synthetic dyes from wastewaters: a review. Environment International, 2004. 30(7): p. 953-971.

[2.] Khan, I., et al., Review on Methylene Blue: Its Properties, Uses, Toxicity and Photodegradation. Water, 2022.

[3.] Yagub, M.T., et al., Dye and its removal from aqueous solution by adsorption: A review. Advances in Colloid and Interface Science, 2014. 209: p. 172-184.

[4.] Low, J., et al., Heterojunction Photocatalysts. Advanced Materials, 2017. 29(20): p. 1601694.

[5.] Fujishima, A., X. Zhang, and D.A. Tryk, TiO2 photocatalysis and related surface phenomena. Surface Science Reports, 2008. 63(12): p. 515-582.

[6.] Samarasinghe, L.V., S. Muthukumaran, and K. Baskaran, Recent advances in visible light-activated photocatalysts for degradation of dyes: A comprehensive review. Chemosphere, 2024. 349: p. 140818.

[7.] Goodarzi, N., et al., Recent progress on semiconductor heterogeneous photocatalysts in clean energy production and environmental remediation. Catalysts, 2023. 13(7): p. 1102.

[8.] Chen, X., L. Guo, and Y. Mao, Semiconductor-Based Photocatalytic Hydrogen Generation. Chemical reviews, 2010. 110: p. 6503-70.

[9.] Li, X., et al., Cocatalysts for Selective Photoreduction of CO 2 into Solar Fuels. Chemical Reviews, 2019. 119.

[10.] Bai, Y., et al., Recent advances in BiVO4-based heterojunction photocatalysts for energy and environmental applications. Chemical Communications, 2025. 61(28): p. 5264-5280.

[11.] Park, Y., K.J. McDonald, and K.-S. Choi, Progress in bismuth vanadate photoanodes for use in solar water oxidation. Chemical Society Reviews, 2013. 42(6): p. 2321-2337.

[12.] Hisatomi, T. and K. Domen, Reaction systems for solar hydrogen production via water splitting with particulate semiconductor photocatalysts. Nature Catalysis, 2019. 2: p. 1.

[13.] Samuel, O., et al., WO3–based photocatalysts: A review on synthesis, performance enhancement and photocatalytic memory for environmental applications. Ceramics International, 2022. 48(5): p. 5845-5875.

[14.] Al-Siani, G. and H.J.J.o.B.E. Kızıltaş, Synthesis and Characterization of BiVO4/WO3/TiO2 Composite for the Photocatalytic Activity of Methylene Blue. 2025. 6(3).

[15.] Balapure, A., J. Ray Dutta, and R. Ganesan, Recent advances in semiconductor heterojunctions: a detailed review of the fundamentals of photocatalysis, charge transfer mechanism and materials. RSC Applied Interfaces, 2024. 1(1): p. 43-69.

[16.] Wang, Q. and K. Domen, Particulate Photocatalysts for Light-Driven Water Splitting: Mechanisms, Challenges, and Design Strategies. Chemical Reviews, 2019. 120.

[17.] Schneider, J., et al., Understanding TiO2 Photocatalysis: Mechanisms and Materials. Chemical reviews, 2014. 114.

[18.] Hong, S., et al., Heterojunction BiVO4/WO3 electrodes for enhanced photoactivity of water oxidation. Energy Environ. Sci., 2011. 4: p. 1781-1787.

[19.] Nie, Z., et al., The Role of Cobalt-Based Cocatalysts on BiVO4 for Photoelectrochemical Water Oxidation. ChemCatChem, 2024. 16.

[20.] Huang, J., et al., Load CoOx cocatalyst on photoanode by spin coating and calcination for enhanced photoelectrochemical water oxidation: A case study on BiVO4. Journal of Solid State Chemistry, 2021. 299: p. 122154.

[21.] Kim, J.H., et al., Carbonate-coordinated cobalt co-catalyzed BiVO4/WO3 composite photoanode tailored for CO2 reduction to fuels. Nano Energy, 2015. 15: p. 153-163.

[22.] Zhang, L., et al., Photodeposited CoO as highly active phases to boost water oxidation on BiVO4/WO3 photoanode. International Journal of Hydrogen Energy, 2019. 44.

[23.] Ran, J., et al., Earth-abundant cocatalysts for semiconductor-based photocatalytic water splitting. Chemical Society Reviews, 2014. 43(22): p. 7787-7812.

[24.] Chen, R., et al., Cocatalysts-Photoanode Interface in Photoelectrochemical Water Splitting: Understanding and Insights. Small, 2024. 20(1): p. e2304807.

[25.] Chugenji, T., Z. Pan, and K. Katayama, Effect of CoO x and Rh Cocatalysts on Local Charge Carrier Dynamics of BiVO 4 Particles by Pattern-Illumination Time-Resolved Phase Microscopy. The Journal of Physical Chemistry C, 2022. 126.

[26.] Omrani, N., A.J.J.o.P. Nezamzadeh-Ejhieh, and P.A. Chemistry, A comprehensive study on the enhanced photocatalytic activity of Cu2O/BiVO4/WO3 nanoparticles. 2020. 389: p. 112223.

[27.] Lv, Y.-R., et al., BiVO4/TiO2 heterojunction with enhanced photocatalytic activities and photoelectochemistry performances under visible light illumination. Materials Research Bulletin, 2019. 117: p. 35-40.

[28.] Yan, X., et al., Converting CoMoO4 into CoO/MoOx for Overall Water Splitting by Hydrogenation. ACS Sustainable Chemistry & Engineering, 2016. 4(7): p. 3743-3749.

[29.] Chen, D., et al., Boosting charge transfer of fe doping BiVO4/CoO x for photoelectrochemical water splitting. 2023. 6(16): p. 8495-8502.

## How to Cite This Article

Hasan, F., Tekin, T., Enhanced Photocatalytic Degradation of Methylene Blue Using a $BiVO_4/WO_3$ Composite Modified with Cobalt-Containing Species, Brilliant Engineering, 4(2026), 41149.
https://doi.org/10.36937/ben.2026.41149